

---

# CalciumGAN: A Generative Adversarial Network Model for Synthesising Realistic Calcium Imaging Data of Neuronal Populations

---

**Bryan M. Li**<sup>1</sup>  
b.m.y.li@sms.ed.ac.uk

**Theoklitos Amvrosiadis**<sup>2</sup>  
t.amvrosiadis@ed.ac.uk

**Nathalie Rochefort**<sup>2,3</sup>  
n.rochefort@ed.ac.uk

**Arno Onken**<sup>1</sup>  
aonken@inf.ed.ac.uk

<sup>1</sup>School of Informatics, University of Edinburgh

<sup>2</sup>Centre for Discovery Brain Sciences, University of Edinburgh

<sup>3</sup>Simons Initiative for the Developing Brain, University of Edinburgh

## Abstract

Calcium imaging has become a powerful and popular technique to monitor the activity of large populations of neurons *in vivo*. However, for ethical considerations and despite recent technical developments, recordings are still constrained to a limited number of trials and animals. This limits the amount of data available from individual experiments and hinders the development of analysis techniques and models for more realistic size of neuronal populations. The ability to artificially synthesize realistic neuronal calcium signals could greatly alleviate this problem by scaling up the number of trials. Here we propose a Generative Adversarial Network (GAN) model to generate realistic calcium signals as seen in neuronal somata with calcium imaging. To this end, we adapt the WaveGAN architecture and train it with the Wasserstein distance. We test the model on artificial data with known ground-truth and show that the distribution of the generated signals closely resembles the underlying data distribution. Then, we train the model on real calcium signals recorded from the primary visual cortex of behaving mice and confirm that the deconvolved spike trains match the statistics of the recorded data. Together, these results demonstrate that our model can successfully generate realistic calcium imaging data, thereby providing the means to augment existing datasets of neuronal activity for enhanced data exploration and modeling.<sup>1</sup>

## 1 Introduction

Recordings of neuronal activities from behaving animals are essential for the study of information processing in the brain. With the advancement of neural recording techniques, such as electrophysiological recordings and calcium imaging, it has become increasingly easier to obtain high quality neuronal activity data *in vivo*. However, due to ethical considerations, the acquired datasets are often limited by the number of trials or the duration of each trial on a live animal. This poses a problem for assessing analysis techniques that take into account higher-order correlations [4, 24–26]. Even for linear decoders, the number of trials can be more important for determining coding accuracy than the number of neurons [27].

---

<sup>1</sup>Code available at [github.com/bryanlimy/calciumgan](https://github.com/bryanlimy/calciumgan)

Generative models of neuronal activity hold the promise of alleviating the above problem by enabling the synthesis of an unlimited number of realistic samples for assessing advanced analysis methods. Recently, the use of deep generative models on neuronal population spike train data has become increasingly popular. Latent Factor Analysis via Dynamical Systems (LFADS, Pandarinath et al. [20]) uses the Variational Autoencoders framework to learn the population dynamics in latent representation (using recurrent neural networks) and extract 'denoised' single-trial firing rates from neural spiking data. Spike-GAN [16] demonstrated that GAN can model neural spikes that accurately match the statistics of real recorded spiking behaviour from a small number of neurons. Moreover, the discriminator in Spike-GAN is able to learn to detect which population activity pattern is the relevant feature, and this can provide insights into how a population of neurons encodes information. Ramesh et al. [21] trained a conditional GAN [15], conditioned on the stimulus, to generate multivariate binary spike trains. They fitted the generative model with recorded data in the V1 area of macaque visual cortex, and GAN generated spike trains were able capture the firing rate and pairwise correlation statistics better than the dichotomized Gaussian model and a deep supervised model.

All of the aforementioned generative models operate on population spike trains. Spike trains are discrete in nature meaning that they cannot be subject to any continuous increment or decrement. Hence it remains a difficult task to optimize deep generative models for discrete data with back-propagation, which is key for training deep neural networks.

Population spike trains can be obtained from different recording techniques, each having advantages and weaknesses. Electrophysiological recordings have high temporal resolution. However, this method is not without flaws [9]. For instance, a single microelectrode can only detect activity from few neurons in close proximity, and extensive pre-processing is required to infer single-unit activity from a multi-unit signal. Disentangling circuit computations in neuronal populations of a large scale remains a difficult task, hence resulting in recordings with low spatial resolution but high temporal resolution [22]. On the other hand, calcium imaging recordings have high spatial resolution and low temporal resolution [28]. This technique, which assesses changes in intracellular calcium concentration as a proxy for neuronal spiking activity, has become a powerful imaging technique to monitor large neuronal populations activity *in vivo*. The continuous nature of calcium fluorescence signals makes optimization via back-propagation a much more straightforward task as compared to spike-train data. Thus, calcium imaging datasets are more attractive candidates for training generative models.

In this work, we explore the feasibility of using the Generative Adversarial Network (GAN) framework to synthesize calcium imaging data, as a method to scale-up or augment the amount of neuronal population activity data. We validate the method on artificial data with known ground-truth and we synthesize data mimicking real two-photon calcium ( $\text{Ca}^{2+}$ ) imaging data as recorded from the primary visual cortex of a behaving mouse [10, 19].

## 2 Methods

### 2.1 Network architecture

The original generative adversarial network framework, introduced by Goodfellow et al. [7], plays a min-max game where the generator  $G$  attempts to generate convincing samples from the latent space  $Z$ , and the discriminator  $D$  learns to distinguish between generated samples and real samples  $X$ . The GAN framework has shown promising results across various domains, such as image and audio generation, unsupervised translation and many more [12, 5, 29]. However, the originally proposed optimization objective was difficult to train, and was prone to mode collapse. Instead of the original objective of minimizing the Jensen-Shannon divergence between the original data distribution and generated data distribution, Arjovsky et al. [1] proposed Wasserstein GAN (WGAN) which minimizes the smoother Earth-Mover's (1st Wasserstein) distance of the two data distributions. In WGAN, the weights of the discriminator (critic) were restricted within a predefined range (weight clipping) in order to enforce the 1-Lipschitz condition and to compute the Wasserstein distance. Gulrajani et al. [8] further improved the objective function with gradient penalty (WGAN-GP), instead of gradient clipping, in order to enforce the Lipschitz condition more effectively. In this work, we use the WGAN-GP formulation of the loss function without the need of incorporating any information of

the neural activities into the objective function:

$$\mathcal{L}_D = \mathbb{E}_{z \sim P_Z} [D(G(z))] - \mathbb{E}_{x \sim P_X} [D(x)] + \lambda \mathbb{E}_{\hat{x} \sim P_{\hat{X}}} [(\|\nabla_{\hat{x}} D(\hat{x})\|_2 - 1)^2]$$

where  $\lambda$  denotes the gradient penalty coefficient and  $\hat{X}$  are samples taken between the true data and generator’s data distribution.

For the network architecture, we adapted the WaveGAN architecture by Donahue et al. [5], which has shown promising results in audio signal generation. The generator uses 1-dimensional transpose convolution layers to up-sample the spatial dimension. Each transpose convolution layer was followed by batch normalization and Leaky ReLU activation. We added a dense layer with sigmoid activation as output layer in the generator. We also replaced Batch Normalization [11] with Layer Normalization [2] in order to make the operation compatible with the WGAN framework. Samples generated using transpose convolution often exhibit the "checkerboard" artifacts described by Odena et al. [18]. In the context of signal generation, the discrimination could exploit the periodic artifacts pattern and learn a naive policy to reject generated samples. Donahue et al. [5] proposed the Phase Shuffle mechanism in the discriminator to address the aforementioned issue. The Phase Shift layer randomly shifts the activated units after each convolution layer by  $-n$  to  $n$  in the time domain, in order to distort the periodic pattern. Hence, the resulting samples constitute a more challenging task for the discriminator. In our network, we incorporated the Phase Shift operation, as well as using a kernel size that is divisible by the stride size, as suggested in Odena et al. [18]. This led to a noticeable improvement in the generated samples. The discriminator is largely a mirror of the generator’s architecture, except for layer normalization which we do not use in the discriminator. Instead, we apply the Phase Shuffle operation after each convolution layer.

To improve the model learning performance and stability, the calcium signals were scaled to the range between 0 and 1 by normalizing with the maximum training set calcium signal. Correspondingly, we chose sigmoid activation in the output layer of the generator and then re-scale the signals to its original range before inferring their spike trains. The model architecture can be found in Table 1.

## 2.2 CalciumGAN Training

We trained both the generator and discriminator with the WGAN framework, with 5 discriminator update steps for each generator update step. We then used Adam optimizer [13] to optimize both networks, with a learning rate of  $\lambda = 10^{-4}$ ,  $\beta_1 = 0.9$  and  $\beta_2 = 0.9999$ . To speed up the training process, we implemented mixed precision training in our codebase. As a result, we are able to train our model with a batch size of 128 on a single NVIDIA RTX 2080 TI GPU. The exact hyper-parameters being used in this work can be found in Table 2.

## 2.3 Spike Train Analysis

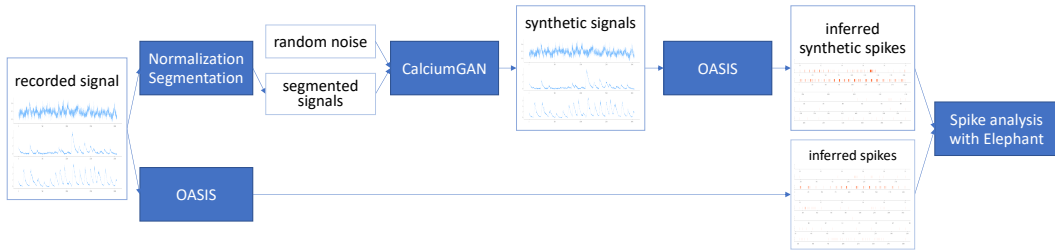


Figure 1: Pipeline diagram of a CalciumGAN analysis. White boxes illustrate data in different processing stages. Blue boxes illustrate analysis steps and techniques.

We devised a consistent model analysis pipeline to evaluate the quality of samples generated by the model, as well as its ability to generalize, in the context of neuronal population spiking activities. The complete model analysis pipeline is shown in Figure 1.

Since we evaluate our model performance in terms of spike activities, we needed a deconvolution algorithm to infer the spike trains from calcium signals. In this work, we used the Online Active

Set method to Infer Spikes (OASIS) deconvolution algorithm [6] for its fast online deconvolution performance.

We apply the Electrophysiology Analysis Toolkit (Elephant, NeuralEnsemble [17]) to measure spike train similarities and statistics. We evaluate the performance of our model with the following spike train statistics and similarities: a) mean firing rate for evaluating single neuron statistics; b) pairwise Pearson correlation coefficient for evaluating pairwise statistics; c) pairwise van-Rossum [23] distance for evaluating general spike train similarity. Importantly, we evaluate these quantities across the whole population for each neuron or neuron pair and each short time interval (100 ms) and compare the resulting distributions over these quantities obtained from training data as well as generated data. We therefore validate the whole spatiotemporal first- and second-order statistics as well as general spike train similarities.

### 3 Results

We propose CalciumGAN as a generative model to synthesize realistic calcium traces as imaged from neuronal populations. To validate our model, we used artificial data with known ground-truth as well as real data recorded from the primary visual cortex of behaving mice.

#### 3.1 Dichotomized Gaussian Training Data

In order to verify that CalciumGAN is able to learn the underlying distribution and statistics of the training data, we generated our own ground-truth dataset with pre-defined mean and covariance using the dichotomized Gaussian (DG) model [14]. The model uses a multivariate normal distribution to generate latent continuous random variables which are then thresholded to generate binary variables representing spike trains. The DG model has mean vector and covariance matrix as free parameters. To generate data from this model, we used the sample means and sample covariances obtained from real recorded data (see Section 3.3). In alignment with the recorded data, we generated correlated spike trains for  $N = 102$  neurons with a duration of 899 seconds and at 24Hz, hence a matrix with shape (21576, 102). In order to obtain calcium-like signals  $c$  from spike trains  $s$  with length  $T$ , we convolved the generated spike trains with a calcium response kernel and added noise, as described in Friedrich et al. [6]:

$$\begin{aligned} s_t &= g \times s_{t-1} + s_t & 1 \leq t \leq T \\ c &= b + s + \sigma u & u \sim \mathcal{N}(0, 1) \end{aligned}$$

where  $g$  denotes a finite impulse response filter,  $b$  is the baseline value of the signal and  $\sigma$  is the noise standard deviation. In our work, we set  $g = 0.95$ ,  $\sigma = 0.3$  and  $b = 0$ . We scale the signals range to 0 to 1. The data is then segmented using a sliding window along the time dimension with a stride of 2 and a window size of  $T = 2048$  (around 85 seconds in experiment time). We apply the segmentation procedure to both the signal and spike data, hence resulting in two matrices with shape (9754, 2048, 102). Examples of signals and spikes generated from the DG model can be found in Figure 7a.

#### 3.2 Synthetic Data Mimicking Dichotomized Gaussian Data

We first fit CalciumGAN to the artificial dataset sampled from the dichotomized Gaussian distribution. We trained CalciumGAN for 400 epochs with 8,754 samples and held out 1,000 samples for evaluation. Since we defined the model from which we generated the training dataset, we can validate the statistics of the dataset generated by CalciumGAN on the known ground-truth directly. Examples of generated signals and spikes can be found in Figure 7b.

We estimated the mean firing rates and the covariances of data generated by CalciumGAN and compared it to the DG ones (Figure 2). We plotted the values of 5 samples for each neuron and neuron-pair, and sorted them by their mean in ascending order. Our model is able to reliably capture the firing rate very well, with root mean square error of 0.0997Hz. The variation of the firing rate across samples matched with those of the ground-truth data. The majority of the neuron pairs have low correlation which was also found in the generated data. The neuron pairs that have highly positive and highly negative covariance also have a greater variation across samples.

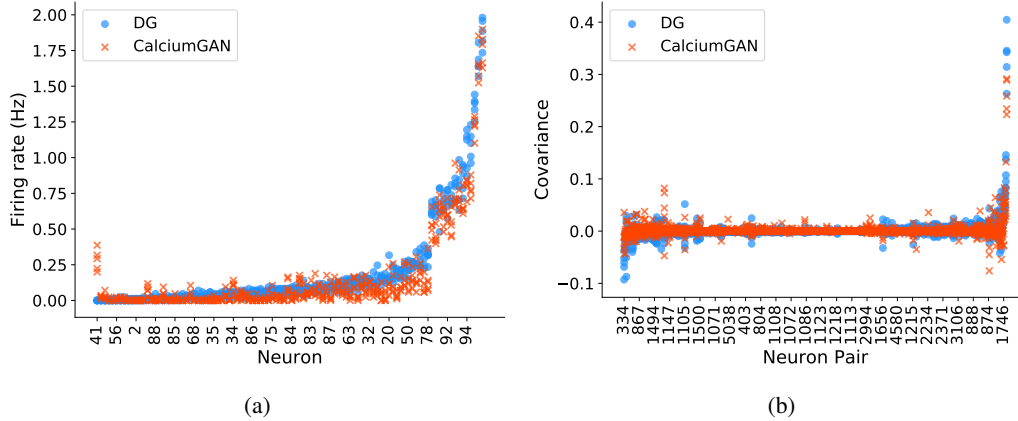


Figure 2: CalciumGAN trained on the dichotomized Gaussian dataset with known ground-truth. (a) Mean firing rate of each neuron. (b) Neuron pairwise covariance. Blue dots represent DG data and orange crosses present generated data. 5 randomly selected samples for each neuron and neuron-pair were displayed in both graphs, where the order on the x-axis was sorted by the mean of the firing rate and covariance respectively. In (b), only every 10<sup>th</sup> pair is displayed, for clarity. Here, we compare both the trend and variation of the generated data statistics with the dichotomized Gaussian data.

### 3.3 Two-photon Calcium Imaging Recorded Data

After validating our model on data with known ground-truth, we applied CalciumGAN on real two-photon calcium imaging data recorded in the primary visual cortex of mice performing a virtual reality task. The data were collected with the same setup as specified in Pagan et al. [19] and Henschke et al. [10]. Head-fixed mice were placed on a cylindrical treadmill, and navigated a virtual corridor rendered on two monitors that covered the majority of their visual field. A lick spout was placed in front of the mice, where a water drop would be made available to the mice as a reward if it licked at the correct location within the virtual environment. Hence, the mice would learn to utilize both the visual information and the self-motion feedback in order to maximize the rewards. Neuronal activity was monitored from the same primary visual cortex populations over multiple consecutive behavioural sessions. In this work, we are using neuron population data recorded on the 4<sup>th</sup> day of the experiment, where the mice were quite familiar with the virtual environment and the given task. In this particular recording, neurons were labelled with GCaMP6f, and  $N = 102$  neurons were recorded at a sampling rate of 24Hz, the mouse performed 204 trials in 898.2 seconds (raw data shape (21556, 102)). Due to the fact that GAN models require a significant amount of training data, information about the trial and position of the mice in the virtual environment were not used in this work.

We applied OASIS AR1 deconvolution algorithm to infer the spike activities from the recorded calcium signals, and performed the same normalization and segmentation steps as mentioned in Section 3.1. Both calcium signals and inferred spike trains have shape (9754, 2048, 102). Figure 3a shows examples of the recorded calcium signals and inferred spike trains. There are multiple challenges for both the generator and discriminator to learn from the calcium imaging signals. Since data were segmented with a sliding window and the information of the trial was not used, some samples might consist of abnormal signal activity, such as a peak being cropped off. Generated signals could have the same number of peaks or ranges, though might not preserve the peak and decay characteristics of calcium imaging data. Real and synthetic activity from less active neurons might be more difficult for the discriminator to distinguish due to the absence of prominent spiking characteristics.

### 3.4 Synthetic Data Mimicking Recorded Data

We tested CalciumGAN with the data recorded from the primary visual cortex of a trained mouse (see Section 3.3). Similar to the DG analysis, we trained the model for 400 epochs, with 8,754 training samples, and 1,000 samples were held out for evaluation. Note that since we are not taking the trial

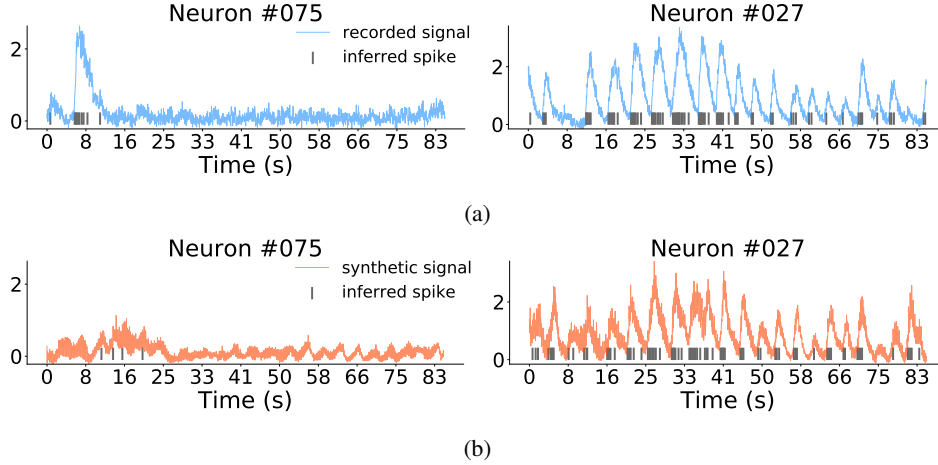


Figure 3: Calcium signals and inferred spike trains (in gray) of randomly selected neurons. (a) shows the recorded data (in blue) and (b) shows synthetic data (in orange) generated by CalciumGAN trained on recorded data. Note that the generated data should not be identical with the recorded data, because CalciumGAN should not replicate the signals and it could generate a sample corresponding to a different trial.

and position of the mice in the virtual environment into consideration when training the model, the generated data and the evaluation data do not have a one-to-one mapping.

We first inspect the generated data and the deconvolved spike trains visually. The calcium signals and inferred spike trains of 6 randomly selected neurons from a randomly selected sample are shown in Figure 3. Both the synthetic raw traces as well as the inferred spikes visually match the characteristics of the recorded ones.

We then compared the spiking characteristics across the whole population. Figure 4 shows the inferred spike trains of the complete 102 neurons population from a randomly selected sample of the real and the synthetic data, with the distribution histogram plotted on the  $x$  and  $y$  axis. The synthetic data mimicks the firing patterns across neurons and across time remarkably well with occasional small deviations in the rates at particular temporal intervals. Notably, the samples are clearly not identical meaning that the network did not just replicate the training set data.

In order to examine if CalciumGAN is able to capture the first and second order statistics of the recorded data, we measured the mean firing rate, pairwise correlation, and van-Rossum distance (see Figure 5). The 3 randomly selected neurons shown in Figure 5a all have very distinct firing rate distributions, and CalciumGAN is able to model all of them relatively well, with KL divergence of 0.42, 0.11 and 0.09 with respect to the recorded firing rate over 1000 samples. We show the pairwise van-Rossum distance of the same neuron between recorded and generated data across 50 samples in Figure 5c as sorted heatmaps. Less active neurons, such as neuron 75, have a low distance value across samples, mainly due to the scarcity of firing events. Conversely, a high frequency neuron, such as neuron 6, exhibits a clear trend of lower distance values in the diagonal of the heatmap, implying the existence of a pair of recorded and generated sample that are similar. In order to ensure that the data generated by our model capture the underlying distribution of the training data, we also compute the KL divergence between the distributions of the above-mentioned metrics (see Figure 6). CalciumGAN was able to model all 3 of the statistics of the recorded data, with most samples having KL divergence values of less than 1.5. Note that we measure the pairwise distance of the same neuron across 50 samples in Figure 5c, whereas in Figure 6c, we measure pairwise van-Rossum distance of each neuron with respect to other neurons within the same sample.

Next, we examined whether CalciumGAN is able to learn from neural activities that are more stochastic and potentially less correlated. To this end, we trained the model on the neuronal populations data recorded on the first day of the mice experiment. Figure 9 shows the raster plot of a randomly selected sample and Figure 11 shows the first and second order statistics of the generated samples, similar to the plots we presented above. Overall, CalciumGAN was able to capture the statistics and

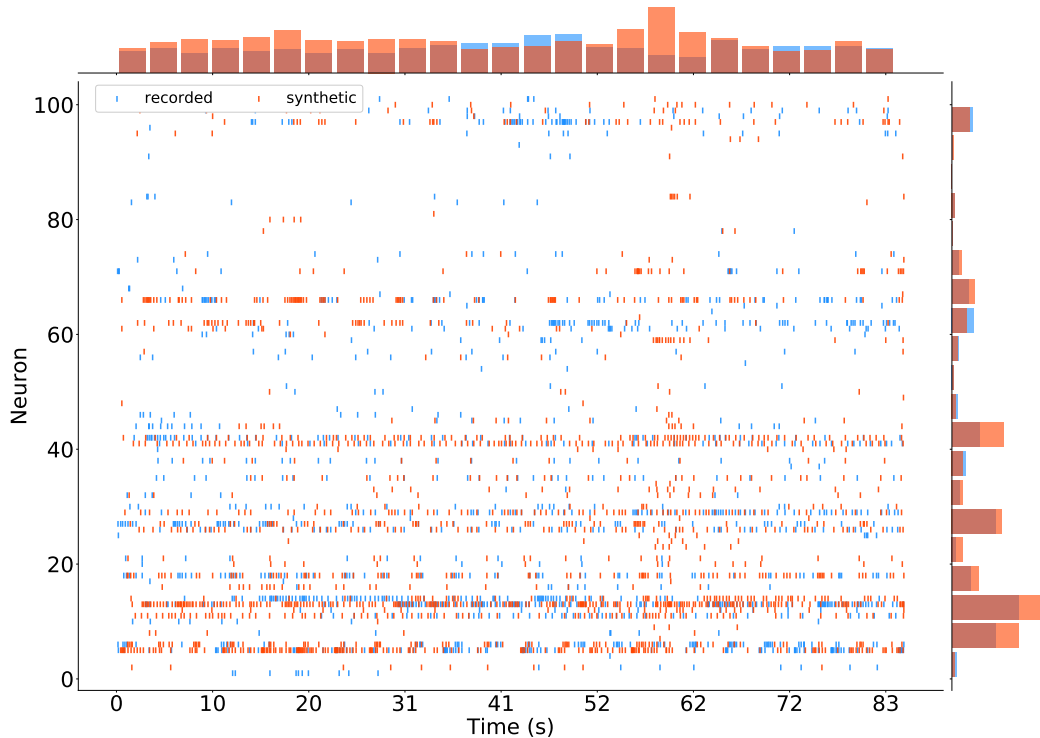


Figure 4: Raster plot of inferred real and synthetic spike trains of a randomly selected sample generated by CalciumGAN trained on recorded data. Blue markers indicate recorded data and orange markers indicate generated data. The histograms on the  $x$  and  $y$  axis indicate number of spikes over the temporal dimension and neuron population respectively.

underlying distribution of the real calcium imaging data acquired in the primary visual cortex of awake, behaving mice.

## 4 Discussion

Despite the recent advancement and popularity of calcium imaging of neuronal activity *in vivo*, the number of trials and the duration of imaging sessions in animal experiments is limited due to ethical and practical considerations. This work provides a readily applicable tool to fit a Generative Adversarial Network model on calcium signals, enabling the generation of more data that matches the statistics of the provided data.

We demonstrated that the GAN framework is capable of synthesizing realistic fluorescent calcium indicator signals similar to those imaged in the somata of neuronal populations of behaving animals. To achieve this, we adapted the WaveGAN [5] architecture with the Wasserstein distance training objective. We generated artificial neuronal activities using a dichotomized Gaussian model, showing that CalciumGAN is able to learn the underlying distribution of the data. We then fitted our model to imaging data from the primary visual cortex of a behaving mice. Importantly, we could show that the statistics of the synthetic spike trains match the statistics of the recorded data.

To infer spike trains from the real and synthetic calcium traces, we used the OASIS deconvolution algorithm, a method which is particularly fast. Speed was a crucial characteristic for evaluating a large number of trials. Nevertheless, we found that this advantage often came at the cost of performance in the form of clearly missed spikes (c.f. Figure 3). However, we stress that these shortcomings apply to both the real data and the synthetic data in exactly the same way. In the end, we use the inferred spikes as a way to validate the plausibility of the synthesized traces. The comparison is fair as long as real and synthetic deconvolutions are subject to the same biases.

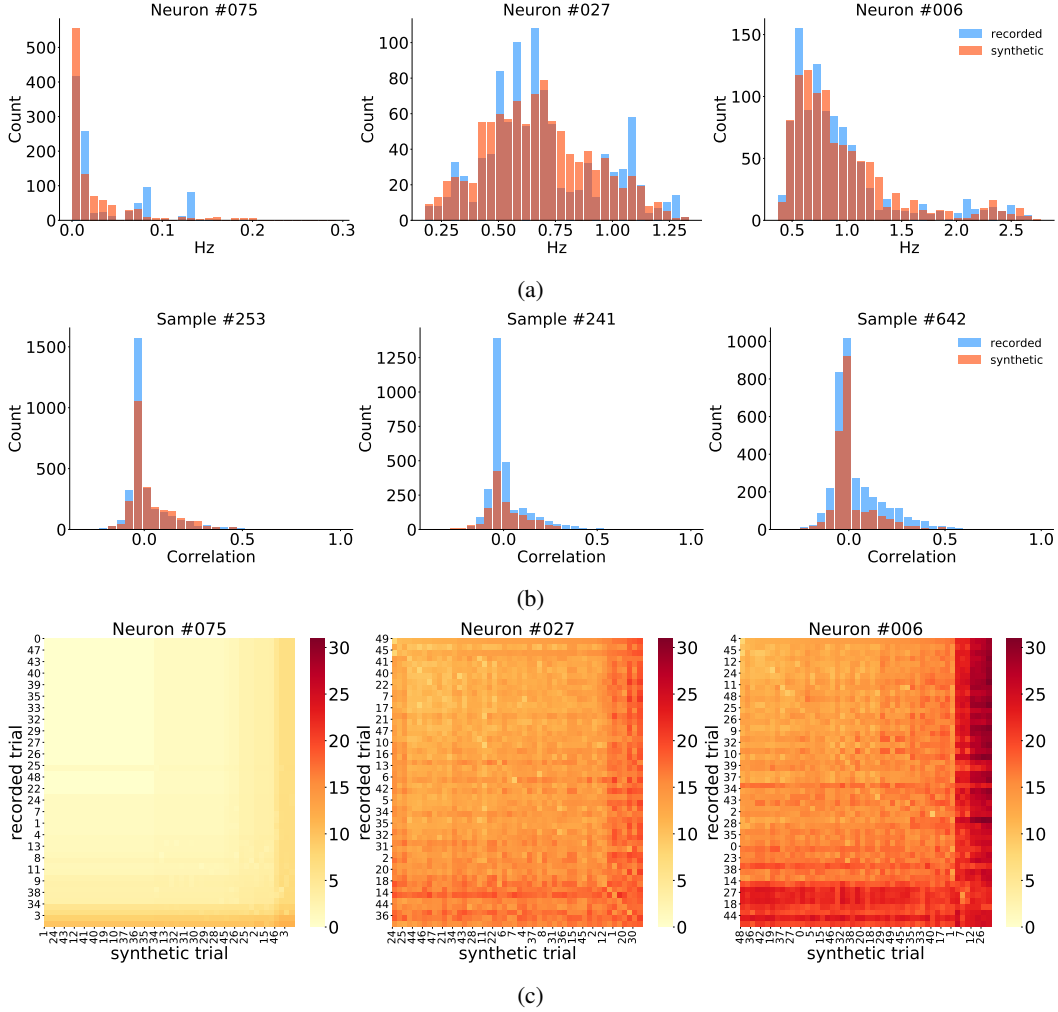


Figure 5: First and second order statistics of data generated from CalciumGAN trained on the recorded data. Shown neurons and samples were randomly selected. (a) Mean firing rate distribution over 1000 samples per neuron. (b) Pearson correlation coefficient distribution. (c) van-Rossum distance between recorded and generated spike trains over 50 samples. Heatmaps were sorted where the pair with the smallest distance value was placed at the top left corner, followed by the pair with the second smallest distance at the second row second column, and so on.

One potential future direction for this work is to provide a meaningful interpretation for the latent generator representation  $z$ . In many image generation tasks with GANs [3, 12] it has been shown that the output image can be modified or targeted by interpolating the latent variable that is fed to the generator. Similarly, one could potentially have final control of the generated calcium signals by exploring the synthetic calcium signals generated after interpolating samples in the latent space. Thereby, one could generate calcium imaging data that resemble the neuronal activities of an animal performing a particular novel task. Another interesting research direction would be using a GAN to learn the relationship between different neuronal populations, or to reveal changes in activity of the same neuronal population in different training phases of an animal learning a behavioral task. This could be achieved by using, for instance, CycleGAN [29], an unsupervised learning model that can learn the mapping between two distributions without paired data, as a potential model architecture.



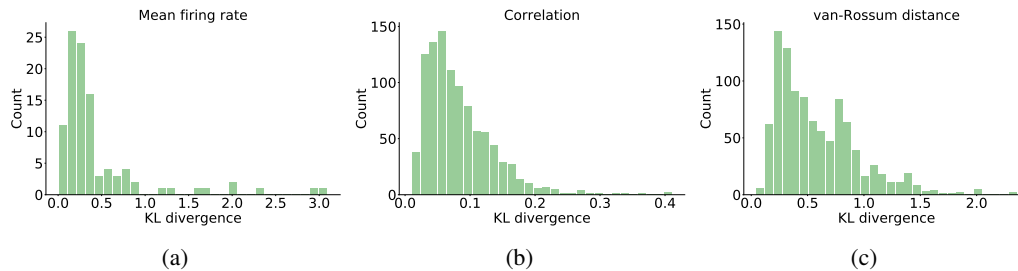


Figure 6: KL divergence of recorded data and generated data distributions. (a) Mean firing rate of each neuron over 1000 trials. (b) Pairwise Pearson correlation coefficient over 1000 trials. (c) Pairwise spike train van-Rossum distance over 1000 trials. The mean KL divergence of each statistics are 0.45, 0.08 and 0.58 respectively.

## Acknowledgments and Disclosure of Funding

We thank the GENIE Program and the Janelia Research Campus, specifically V. Jayaraman, R. Kerr, D. Kim, L. Looger, and K. Svoboda, for making GCaMP6 This work was funded by the Engineering and Physical Sciences Research Council (grant EP/S005692/1 to A.O.), the Wellcome Trust and the Royal Society (Sir Henry Dale fellowship to N.R.), the Marie Curie Actions of the European Union’s FP7 program (MC-CIG 631770 to N.R.), the Simons Initiative for the Developing Brain (to N.R.), the Precision Medicine Doctoral Training Programme (MRC, the University of Edinburgh (to T.A.)).

## References

- [1] Martin Arjovsky, Soumith Chintala, and Léon Bottou. Wasserstein gan. *arXiv preprint arXiv:1701.07875*, 2017.
- [2] Jimmy Lei Ba, Jamie Ryan Kiros, and Geoffrey E Hinton. Layer normalization. *arXiv preprint arXiv:1607.06450*, 2016.
- [3] Piotr Bojanowski, Armand Joulin, David Lopez-Paz, and Arthur Szlam. Optimizing the latent space of generative networks. *arXiv preprint arXiv:1707.05776*, 2017.
- [4] Emery N Brown, Robert E Kass, and Partha P Mitra. Multiple neural spike train data analysis: state-of-the-art and future challenges. *Nature neuroscience*, 7(5):456–461, 2004.
- [5] Chris Donahue, Julian McAuley, and Miller Puckette. Adversarial audio synthesis. In *International Conference on Learning Representations*, 2019. URL <https://openreview.net/forum?id=ByMVTsR5KQ>.
- [6] Johannes Friedrich, Pengcheng Zhou, and Liam Paninski. Fast online deconvolution of calcium imaging data. *PLoS computational biology*, 13(3):e1005423, 2017.
- [7] Ian Goodfellow, Jean Pouget-Abadie, Mehdi Mirza, Bing Xu, David Warde-Farley, Sherjil Ozair, Aaron Courville, and Yoshua Bengio. Generative adversarial nets. In Z. Ghahramani, M. Welling, C. Cortes, N. D. Lawrence, and K. Q. Weinberger, editors, *Advances in Neural Information Processing Systems 27*, pages 2672–2680. Curran Associates, Inc., 2014. URL <http://papers.nips.cc/paper/5423-generative-adversarial-nets.pdf>.
- [8] Ishaan Gulrajani, Faruk Ahmed, Martin Arjovsky, Vincent Dumoulin, and Aaron C Courville. Improved training of wasserstein gans. In *Advances in neural information processing systems*, pages 5767–5777, 2017.
- [9] Kenneth D Harris, Rodrigo Quian Quiroga, Jeremy Freeman, and Spencer L Smith. Improving data quality in neuronal population recordings. *Nature neuroscience*, 19(9):1165, 2016.
- [10] Julia U Henschke, Evelyn Dylda, Danai Katsanevaki, Nathalie Dupuy, Stephen P Currie, Theoklitos Amvrosiadis, Janelle MP Pakan, and Nathalie L Rochefort. Reward association enhances stimulus-specific representations in primary visual cortex. *Current Biology*, 2020.

- [11] Sergey Ioffe and Christian Szegedy. Batch normalization: Accelerating deep network training by reducing internal covariate shift. *arXiv preprint arXiv:1502.03167*, 2015.
- [12] Tero Karras, Timo Aila, Samuli Laine, and Jaakko Lehtinen. Progressive growing of gans for improved quality, stability, and variation. *arXiv preprint arXiv:1710.10196*, 2017.
- [13] Diederik P Kingma and Jimmy Ba. Adam: A method for stochastic optimization. *arXiv preprint arXiv:1412.6980*, 2014.
- [14] Jakob H Macke, Philipp Berens, Alexander S Ecker, Andreas S Tolias, and Matthias Bethge. Generating spike trains with specified correlation coefficients. *Neural computation*, 21(2): 397–423, 2009.
- [15] Mehdi Mirza and Simon Osindero. Conditional generative adversarial nets. *arXiv preprint arXiv:1411.1784*, 2014.
- [16] Manuel Molano-Mazon, Arno Onken, Eugenio Piasini\*, and Stefano Panzeri\*. Synthesizing realistic neural population activity patterns using generative adversarial networks. In *International Conference on Learning Representations*, 2018. URL <https://openreview.net/forum?id=r1VVsebAZ>.
- [17] NeuralEnsemble. Elephant. URL <https://github.com/NeuralEnsemble/elephant>.
- [18] Augustus Odena, Vincent Dumoulin, and Chris Olah. Deconvolution and checkerboard artifacts. *Distill*, 2016. doi: 10.23915/distill.00003. URL <http://distill.pub/2016/deconv-checkerboard>.
- [19] Janelle MP Pakan, Stephen P Currie, Lukas Fischer, and Nathalie L Rochefort. The impact of visual cues, reward, and motor feedback on the representation of behaviorally relevant spatial locations in primary visual cortex. *Cell reports*, 24(10):2521–2528, 2018.
- [20] Chethan Pandarinath, Daniel J O’Shea, Jasmine Collins, Rafal Jozefowicz, Sergey D Stavisky, Jonathan C Kao, Eric M Trautmann, Matthew T Kaufman, Stephen I Ryu, Leigh R Hochberg, et al. Inferring single-trial neural population dynamics using sequential auto-encoders. *Nature methods*, page 1, 2018.
- [21] Poornima Ramesh, Mohamad Atayi, and Jakob H Macke. Adversarial training of neural encoding models on population spike trains. 2019.
- [22] Hernan Gonzalo Rey, Carlos Pedreira, and Rodrigo Quian Quiroga. Past, present and future of spike sorting techniques. *Brain research bulletin*, 119:106–117, 2015.
- [23] MCW van Rossum. A novel spike distance. *Neural computation*, 13(4):751–763, 2001.
- [24] Shreya Saxena and John P. Cunningham. Towards the neural population doctrine, 2019. ISSN 18736882.
- [25] Benjamin Staude, Stefan Rotter, and Sonja Grün. Cubic: cumulant based inference of higher-order correlations in massively parallel spike trains. *Journal of computational neuroscience*, 29(1-2):327–350, 2010.
- [26] Ian H. Stevenson and Konrad P. Kording. How advances in neural recording affect data analysis. *Nature Neuroscience*, 14(2):139–142, feb 2011. ISSN 1097-6256. doi: 10.1038/nn.2731. URL <http://www.nature.com/articles/nn.2731>.
- [27] Carsen Stringer, Michalis Michaelos, and Marius Pachitariu. High precision coding in visual cortex. *bioRxiv*, 2019. doi: 10.1101/679324. URL <https://www.biorxiv.org/content/early/2019/11/04/679324>.
- [28] Ziqiang Wei, Bei-Jung Lin, Tsai-Wen Chen, Kayvon Daie, Karel Svoboda, and Shaul Druckmann. A comparison of neuronal population dynamics measured with calcium imaging and electrophysiology. *bioRxiv*, page 840686, 2019.
- [29] Jun-Yan Zhu, Taesung Park, Phillip Isola, and Alexei A Efros. Unpaired image-to-image translation using cycle-consistent adversarial networks. In *Proceedings of the IEEE international conference on computer vision*, pages 2223–2232, 2017.

## Supplementary material

Table 1: The generator (a) and discriminator (b) architecture of CalciumGAN. The generator consists of 4,375,740 parameters, and the discriminator consists of 4,110,273 parameters.

Layer	Output shape	Layer	Output shape
Input	(n, 32)	Input	(n, 2048, 102)
Dense	(n, 2048)	Conv1D	(n, 1024, 64)
LeakyRelu	(n, 2048)	LeakyRelu	(n, 1024, 64)
Reshape	(n, 64, 32)	PhaseShift	(n, 1024, 64)
Conv1DTranspose	(n, 128, 320)	Conv1D	(n, 512, 128)
LayerNorm	(n, 128, 320)	LeakyRelu	(n, 512, 128)
LeakyRelu	(n, 128, 320)	PhaseShift	(n, 512, 128)
Conv1DTranspose	(n, 256, 256)	Conv1D	(n, 256, 192)
LayerNorm	(n, 256, 256)	LeakyRelu	(n, 256, 192)
LeakyRelu	(n, 256, 256)	PhaseShift	(n, 256, 192)
Conv1DTranspose	(n, 512, 192)	Conv1D	(n, 128, 256)
LayerNorm	(n, 512, 192)	LeakyRelu	(n, 128, 256)
LeakyRelu	(n, 512, 192)	PhaseShift	(n, 128, 256)
Conv1DTranspose	(n, 1024, 128)	Conv1D	(n, 64, 320)
LayerNorm	(n, 1024, 128)	LeakyRelu	(n, 64, 320)
LeakyRelu	(n, 1024, 128)	Flatten	(n, 20480)
Conv1DTranspose	(n, 2048, 102)	Dense	(n, 1)
LayerNorm	(n, 2048, 102)		
LeakyRelu	(n, 2048, 102)		
Dense	(n, 2048, 102)		
Sigmoid	(n, 2048, 102)		

(b) Discriminator architecture

(a) Generator architecture

Table 2: CalciumGAN hyperparameters

Hyper-parameters	Value
Filters	64
Kernel size	24
Stride	2
Noise dimension	32
Critic update	5
$\lambda$ gradient penalty	10
Batch size	128
Epochs	400
Learning rate	0.0001
Phase shift	10

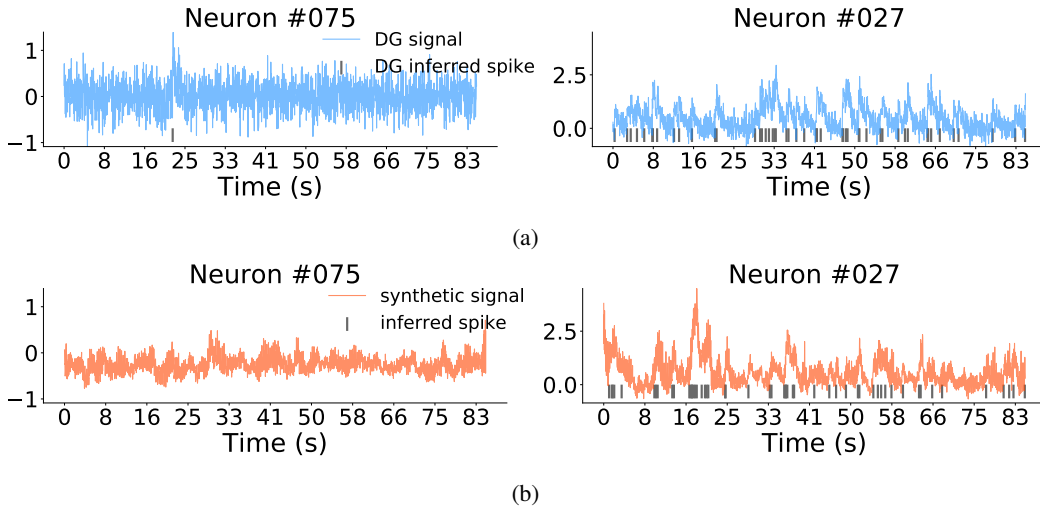


Figure 7: Calcium signals and inferred spike trains (in gray) of randomly selected neurons. (a) shows the dichotomized Gaussian data (in blue) and (b) shows synthetic data (in orange) generated by CalciumGAN trained on the DG data. Notice that the artificial signal data transformed from DG spike data (see Section 3.1) do not have the peak and decay characteristics of typical calcium imaging data.

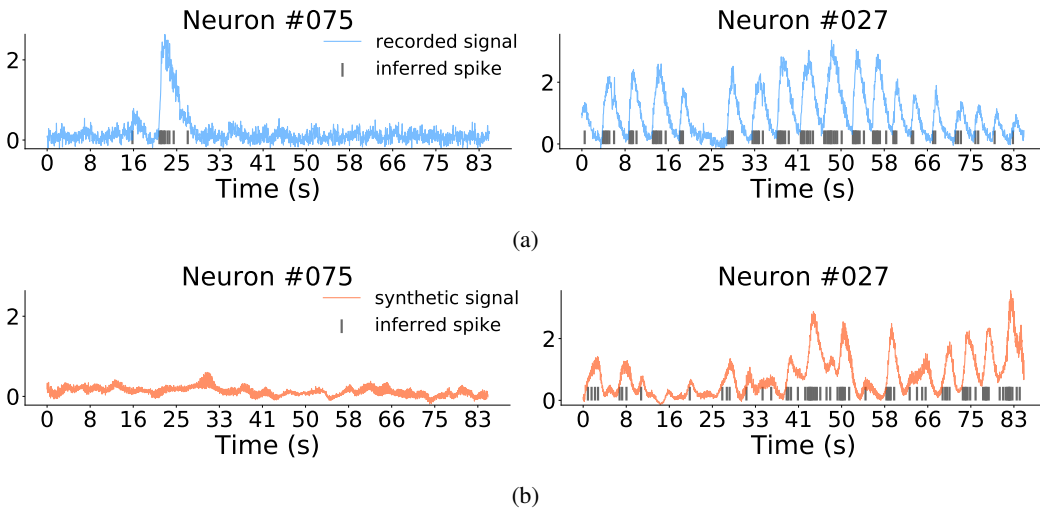


Figure 8: Calcium signals and inferred spike trains (in gray) of randomly selected neurons. (a) shows the recorded data (in blue) and (b) shows synthetic data (in orange) generated by CalciumGAN trained on the recorded data with no Phase Shift (see Section 2.1). Notice the sharp rise to peak followed by a tail of decaying signal which is outside of the window shown for CalciumGAN.

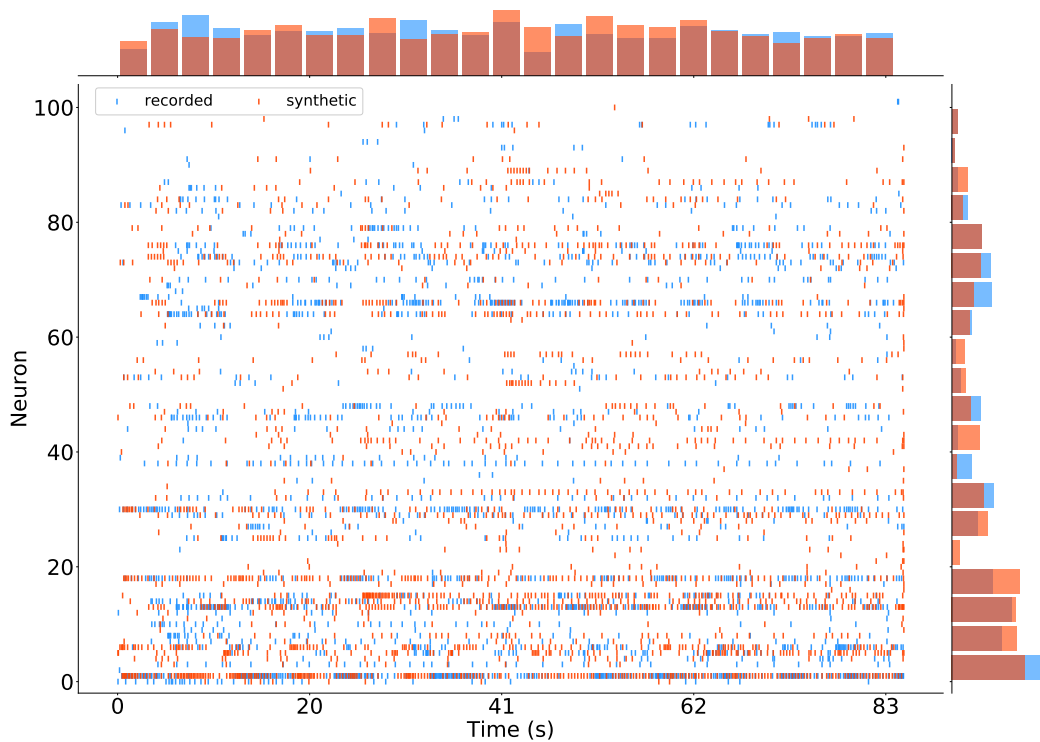


Figure 9: Raster plot of inferred real and synthetic spike trains of a randomly selected sample generated by CalciumGAN trained on calcium imaging data recorded on day one of the animal experiment. Blue markers indicate recorded data and orange markers indicate generated data. The histograms on the  $x$  and  $y$  axis indicate number of spikes over the temporal dimension and neuron population respectively. Compared to recordings acquired on the 4<sup>th</sup> day of the experiment, most neurons recorded in the untrained animal are more active.

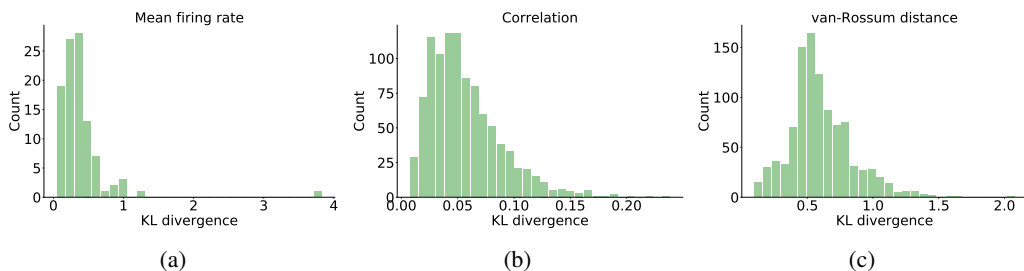


Figure 10: KL divergence of calcium data recorded on day 1 of the animal experiment and generated data distributions. (a) Mean firing rate of each neuron over 1000 trials. (b) Pairwise Pearson correlation coefficient over 1000 trials. (c) Pairwise spike train van-Rossum distance over 1000 trials. The mean KL divergence of each statistics are 0.38, 0.06 and 0.60 respectively.

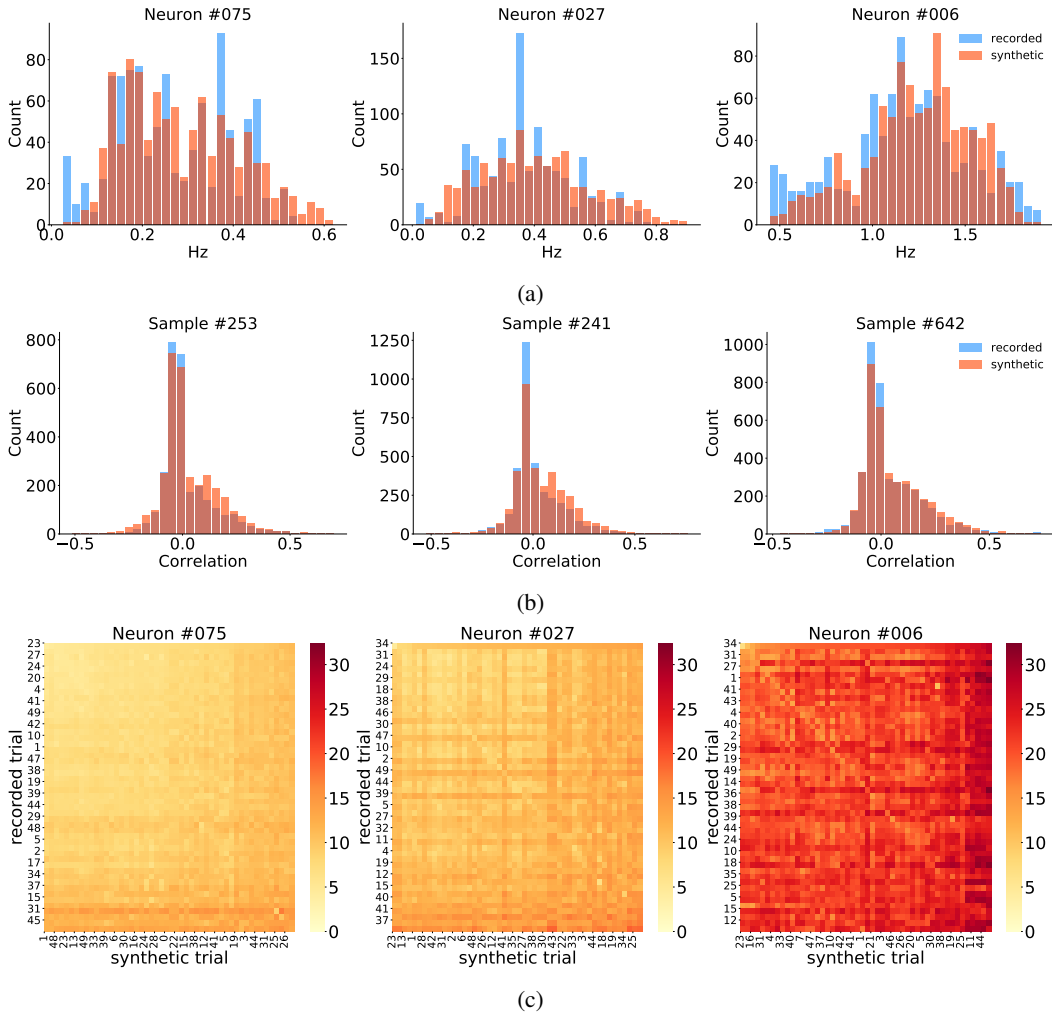


Figure 11: First and second order statistics of data generated from CalciumGAN trained on calcium imaging data recorded on day one of the animal experiment. Shown neurons and samples were randomly selected. (a) Mean firing rate distribution over 1000 samples per neuron. (b) Pearson correlation coefficient distribution. (c) van-Rossum distance between recorded and generated spike trains over 50 samples. Heatmaps were sorted where the pair with the smallest distance value was placed at the top left corner, followed by the pair with the second smallest distance at the second row second column, and so on.